Research Square

Preprints are preliminary reports that have not undergone peer review.
They should not be considered conclusive, used to inform clinical practice,
or referenced by the media as validated information.

A DNS display of stronger centrifugal velocity in rotational axisymmetric turbulence

Samuel David Dunstan

samueld.dunstan@gmail.com

The Papua New Guinea University of Technology https://orcid.org/0000-0002-7738-2401

Research Article

Keywords: rotational frame, centripetal velocity, divergence theorem, Stokes theorem, third central moment.

Posted Date: April 21st, 2026

DOI: https://doi.org/10.21203/rs.3.rs-9467877/v1

License: This work is licensed under a Creative Commons Attribution 4.0 International License.
Read Full License

Additional Declarations: The authors declare no competing interests.

A DNS display of stronger centrifugal velocity in rotational axisymmetric turbulence

Samuel D. Dunstan[1] [2]
[1]School of Engineering, University of Warwick, Coventry CV4 7AL, UK
[2]The Papua New Guinea University of Technology

Abstract

It is not new knowledge that when fluids undergo rotation, "fictitious forces" are introduced, the Coriolis force and centrifugal force. It is often interpreted that these fictitious forces occur due to consideration of the physics in the rotational reference frame. In Dunstan (2023) it was shown that in rotating axisymmetric turbulence, particularly in a concentric pipe with inner wall rotating, that regardless of the frame of the observer, the turbulent fluid behaves according to Coriolis motion dictated by observation in the rotating reference frame. It has also been known for a long time (eg. Einstein's tea-leaf paradox discussion (Barkley (2020)) that fluids under rotation exhibit centrifugal force, which is also often attributed to fluid behaviour in the rotational frame. In the following paper we show that numerical experiments indicate that no matter the reference frame of the observer, "centrifugal" (outward radial) velocity appears to be stronger than "centripetal" (inward radial) velocity. The constraints of the continuity equation are considered. An attempt is made to equate the Gauss' (divergence) theorem to Stokes (circulation) theorem, via the third moment of fluctuating radial velocity.

1 Introduction

1.1 Invariance of instantaneous fluctuating velocity

Firstly, it needs to be emphasized that to compare physical behaviour in different reference frames an invariant quantity needs to be identified and used. To this end, as in Dunstan

(2023) we utilize the fluctuating velocity of turbulence, which we find to be a suitable invariant in the context of these discussions. The proof of the invariance of fluctuating velocity has been derived by Speziale (1979) and is given in Appendix A.

1.2 Derivation of the continuity equation

The restrictions of the continuity equation $\nabla \cdot \mathbf{u} = 0$ in bounded incompressible axisymmetric turbulence (pipe turbulence), means that there cannot be any source or sink for radial velocity v_r terms in such enclosed conduits, and this also applies to ensemble fluctuating radial velocity $\overline{v_r'}$.

For clarity we take a step back and consider the derivation of the continuity equation, beginning with mass conservation in a volume,

$$m = \iiint_V \rho \, dV$$

then consider the flux through the volume, and the Gauss (divergence) theorem,

$$\frac{d}{dt} \iiint_V \rho \, dV = - \iint_\sigma \rho \mathbf{F} \cdot \mathbf{n} \, dS = \iiint_V \nabla \cdot (\rho \mathbf{F}) \, dV$$
$$\therefore \iiint_V \left(\frac{\partial \rho}{\partial t} + \nabla \cdot (\rho \mathbf{F}) \right) dV = 0$$

which means,

$$\frac{\partial \rho}{\partial t} + \nabla \cdot (\rho \mathbf{F}) = 0$$
$$= \frac{\partial \rho}{\partial t} + \rho (\nabla \cdot \mathbf{F}) + (\nabla \rho) \cdot \mathbf{F} \qquad \text{(by the chain rule).}$$

In incompressible flows, where density is considered constant,

$$\nabla \cdot \mathbf{F} = 0.$$

In pipes and other axisymmetric conduits, polar coordinates can be applied and the

continuity equation is given as,

$$\frac{1}{r}\frac{\partial r u_r}{\partial r} + \frac{1}{r}\frac{\partial u_\theta}{\partial \theta} + \frac{\partial u_z}{\partial z} = 0$$

1.3 Thought experiment

Consider the following thought experiment on radial velocity in an axisymmetric cross-sectional surface for turbulent flow in a concentric pipe or pipe, as shown in Figure 1. For

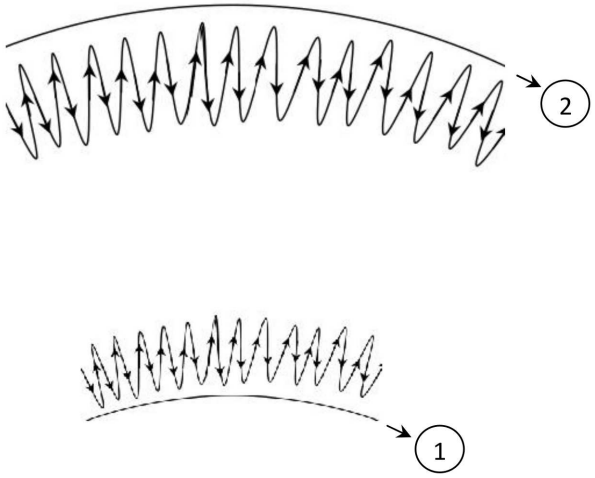


Figure 1: Caricature of possible (idealised) fluctuating radial velocity $v_r^{'}$ patterns in an axisymmetric cross-section

centripetal/centrifugal force in a confined flow, there is also the dilemma of continuity, i.e. we cannot have unidirectional radial velocity. Therefore the arrows of the radial velocity vector field must be in opposing directions to have a net zero resultant.

In this figure ① is a caricature of the inner rotating wall of a concentric pipe, while the ② could be for either the outer wall or a pipe-wall. In these sketches the arrows are not purely radial. Now consider if the arrows were purely radial (inward/ outward) and hence not joined. At the pipe centre, one could reason that, of the two directions there would have to be a stronger direction; either inwards (centripetal) or outwards (centrifugal), this stronger direction would continue all the way to the centre. Due to continuity the weaker direction could be more numerous, so net value is still zero. The question now is how do we determine which direction is stronger, centripetal or centrifugal? One answer is to take a measurement of the third moment of fluctuating radial velocity - also known

as the skewness of fluctuating radial velocity. This has been done in the following DNS simulation.

2 Numerical simulation computational details

The `nek5000` DNS solver (by Fischer et al. (2008)) was used by Dunstan (2023) and the full record of all direct numerical simulation (DNS) experiments done is detailed in Dunstan (2020). Rotational turbulence was studied in four different axisymmetric geometries; the pipe, concentric pipe with inner wall rotating, concentric pipe with outer wall rotating and the pipe-jet under Coriolis rotation. Due to time constraints, statistical stationarity was only reasonably achieved in the pipe and largely achieved in the concentric pipe with inner wall rotating. The flow was still being developed in the concentric pipe with outer wall rotating and in the pipe-jet under Coriolis rotation.

This paper seeks to utilize results obtained from the pipe and concentric pipe with inner rotating wall simulations. `nek5000` intends to solve the incompressible, isothermal and nondimensional Navier-Stokes equations at every timestep for all turbulent motions down to the Kolmogorov scale for the;
continuity equations:

$$\nabla \cdot \mathbf{u} = 0 \tag{1}$$

and, momentum equations:

$$\mathbf{u}_t + (\mathbf{u} \cdot \nabla)\mathbf{u} = -\nabla p + \frac{1}{Re}\Delta \mathbf{u} + \mathbf{f} \tag{2}$$

where Re is Reynolds number and Δ is the Laplacian.

2.1 Geometry and flow parameters

The geometry, flow parameters and validation results for the pipe and concentric pipe have already been fully outlined in Dunstan (2023) and Dunstan (2020) and will not be repeated here. Throughout this paper the rotation rate is quantified by N, the ratio of

mean azimuthal velocity (U_θ) to mean streamwise velocity (U_z). Here U are velocities in the inertial frame while V are in the rotational frame (with only V_θ being different).

3 Results and discussion

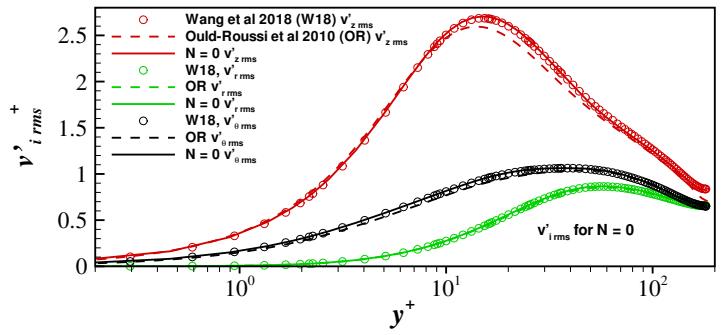
3.1 The pipe under rotation

Having established in Dunstan (2023) that in rotational turbulence the fluid orientation is Coriolis in nature and therefore azimuthal velocity v_θ has to be examined in the rotating reference frame. The plot for time averaged azimuthal velocity has already been given in Dunstan (2023) therefore will not be given in the main text here again but can be found in a side-by-side comparison in Appendix B.1

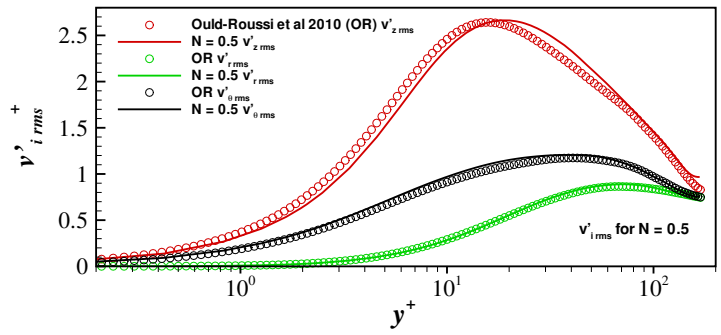
3.2 Pipe flow validation

Other mean flow characteristics such as streamwise velocity and the superimposed validation plots can also be found in Dunstan (2020, 2023). However seeing as validation is such a critical step in numerical simulations, the $v_{i\,rms}$ plots are given here in Figure 2.

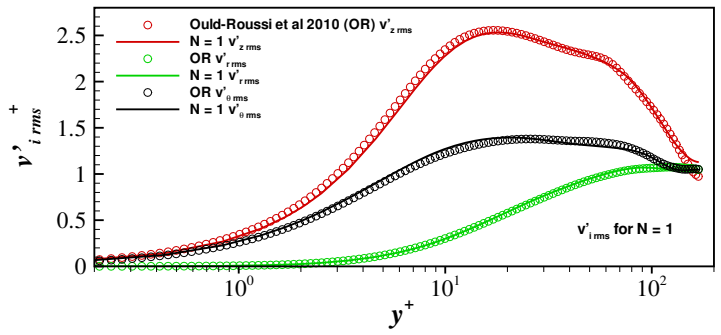
The $v_{i\,rms}$ data from Ould-Rouiss et al. (2010), in wall units, obtained from the authors of Mullyadzhanov et al. (2017), is plotted against the current results and there is generally good agreement for all cases. For the $N = 0$ case a comparison is made with the `nek5000` obtained DNS data of Wang (2017). This data from Wang (2017) was obtained using `nek5000` polynomial order $\mathcal{N} = 9$. In comparing with the current $N = 0$ pipe data at same axial $Re_\tau = 180$ but at `nek5000` $\mathcal{N} = 7$, there is exact coincidence of the plots. Hence this check essentially also serves as a grid sensitivity check for this pipe mesh. For the $N = 0$ case, only the plot for $v'_{z,\,rms}$ for Ould-Rouiss et al. (2010) deviates slightly at mid pipe-radius. This persists for the $N = 0.5$ case, however at $N = 1$ there is good coincidence. Presumably this is because three-dimensional turbulence has been reduced and the mesh of Ould-Rouiss et al. (2010) is now sufficiently resolved.



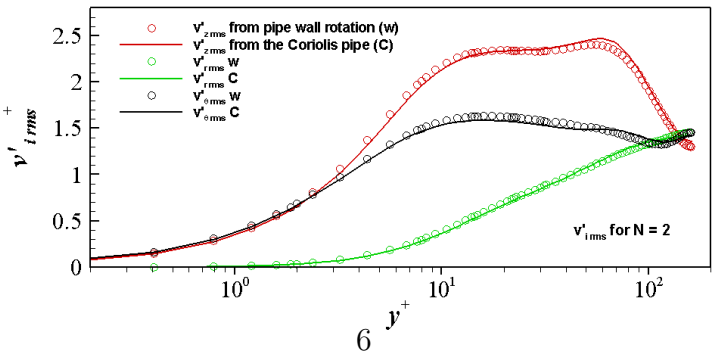
(a)



(b)



(c)



(d)

Figure 2: v_i' $_{rms}$ velocity profile for the axially rotating pipe at rotating rate (a) $N = 0$, (b) $N = 0.5$, (c) $N = 1$, (d) $N = 2$.

3.2.1 Pipe skewness or third moment of $v_r^{'}$

In the opening remarks of White (1964), stability in the flow due to rotation occurs when angular momentum increases with radius, such as that which occurs in the rotating pipe. Per White (1964), in this situation the balance between centrifugal (rotating reference frame) and centripetal (inertial reference frame) forces occurs and hence radial motions are suppressed Kikuyama et al. (1983); Reich and Beer (1989); White (1964). These demonstrations can be seen in the pipe with wall rotation in Figure 6, and in the concentric pipe with outer wall rotating (see Figure 8 in the Appendix). Whilst there is no net mean radial flow due to the restriction of the continuity equation, it is possible, via the third moment of v_r', also called skewness, (normalized by a convenient quantity to make dimensionless $\overline{v_r'^3}/\overline{(v_r'^2)^{3/2}}$), to examine where in the pipe section is the strength of inward (centripetal) wall-normal positive flow, or outward (centrifugal) negative flow, more dominant. Plots for this are done in Figure 3 to examine this. Since turbulence manifests in the rotational reference frame (Dunstan (2023)), it is expected that with increased rotation there will be high centrifugal action, as opposed to centripetal action encountered with rotation in the inertial reference frame.

As expected, as N increases to 2 in the pipe with wall rotation, there is higher strength of outward (negative) third moment of velocity fluctuations. To clarify, the simulations are done in line with one of the earliest credible DNS simulations by Kim et al. (1987) (KMM), where the wall-normal direction, away from the (lower) wall (in KMM), is positive. Therefore from Figure 3 as the rotation rate approaches $N = 2$ there is an increased strength of centrifugal (outward negative) third-moment of radial velocity fluctuations. Generally, this increased radial velocity fluctuation is seen to contributed to turbulent kinetic energy (TKE) as well (Dunstan (2020)). This is shown in Figure 4, where despite the belief that "relaminarisation" or increased stability or two-dimensionalisation occurs in a turbulent pipe with rotation, there is in fact increased TKE. This has been pointed out in early DNS studies into the rotating turbulent pipe (eg. Orlandi and Fatica (1997)).

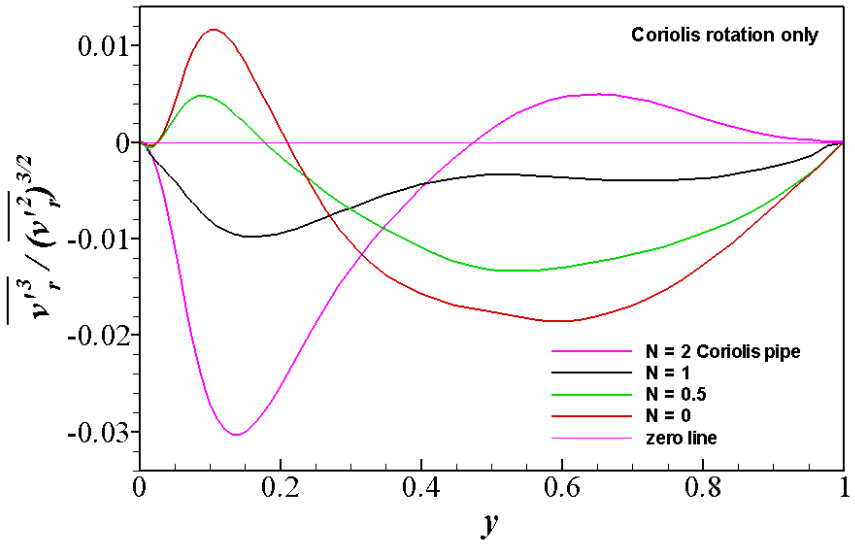


Figure 3: Radial skewness in the pipe with rotation

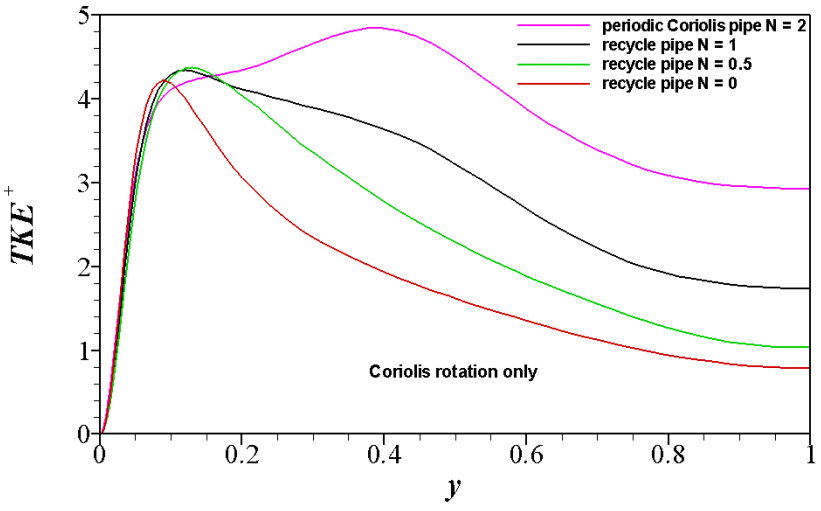


Figure 4: Turbulent kinetic energy in the pipe with rotation

3.3 The concentric pipe under rotation

As discussed earlier, statistical stationarity in the concentric pipe with inner wall rotating was largely established. In Dunstan (2023) it has been elaborated that the geometry for the concentric pipe with inner wall rotating was finely resolved and hence good fidelity validation of results was obtained and detailed.

3.3.1 Skewness and kurtosis

From the plots of Coriols azimuthal velocity in Dunstan (2023), high clockwise (negative) rotation occurs near the inner wall (near $y = 0.05$). Here there is a corresponding increase in positive, wall-normal (away from the inner wall), third moment of $v_r^{'}$, radial velocity fluctuations. The plot for v_r' skewness for $N = 0$ is very similar to that in the channel as shown by KMM (Kim et al. (1987)), and shown here in Figure 9 in Appendix C. In Figure 5, at $N = 0$, v_r' skewness on the inner and outer wall show prominently positive and negative radial velocity fluctuations respectively, which correspond to prominent ejections from either wall, normally encountered in a two dimensional turbulent boundary layer (2DTBL). Figure 5 shows how the natural positive (outward) skewness tendency at $N = 0$ is then enhanced, by the clockwise Coriolis rotation which manifests near the inner rotating wall. Here outward positive (centrifugal) skewness of velocity fluctuations increases with rotation, hence enhanced ejections and compensating splatting, which leads to an increase in three-dimensional turbulence, brought about by rotation of the inner wall. Figure 5 is essentially a raw demonstration of centrifugal force in fluid flow, not dissimilar to that discussed in the *tea-leaf* paradox, which occurs towards the surface of the tea-cup. Chung and Sung (2005) and others have shown corresponding high magnitude negative pressure strain on the inner rotating wall of the concentric pipe.

4 Discussion

Clearly by taking the third moment of fluctuating radial velocity it can be seen that centrifugal velocity is stronger in the pipe with wall rotation and in the concentric pipe with inner wall rotation.

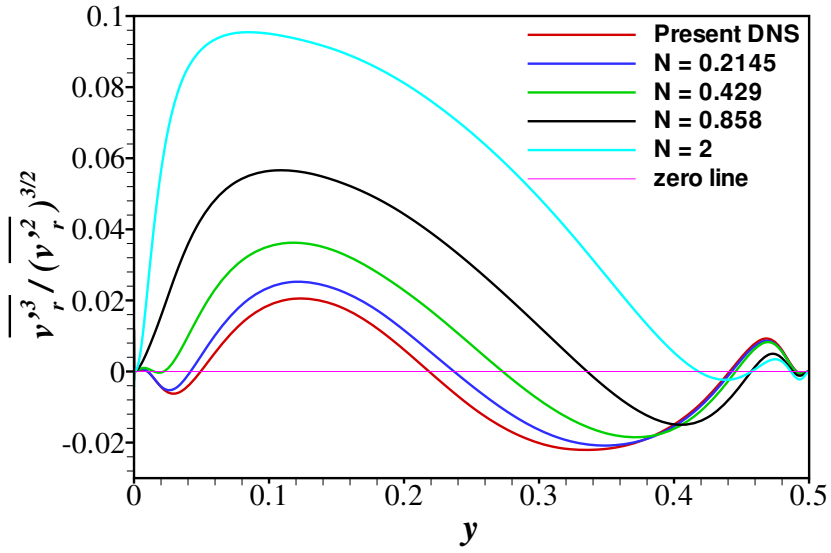


Figure 5: Radial skewness in the concentric pipe with rotation.

Now consider the Stokes theorem which has to do with circulation

$$\oint_C \mathbf{F} \cdot \mathbf{T}\, ds = \oint_C \mathbf{F} \cdot d\mathbf{r} = \iint_\sigma (\text{curl}\ \mathbf{F}) \cdot \mathbf{n}\, dS \tag{3}$$

Now both the Gauss theorem, which is the source of the continuity equation and the Stokes theorem can be derived from the generalized Stokes theorem

$$\int_\Omega d\omega = \int_{\partial\Omega} \omega \tag{4}$$

However it is impossible to directly equate Gauss theorem to Stokes theorem, i.e. respectively,

$$\left(\int_V (\nabla \cdot \mathbf{F})\, dV = \oint_{\partial V} \mathbf{F} \cdot d\mathbf{A} \right) \neq \left(\oint_{\partial S} \mathbf{F} \cdot d\boldsymbol{\ell} = \int_S (\nabla \times \mathbf{F}) \cdot d\mathbf{A} \right) \tag{5}$$

Obviously in the described DNS experiments there is direct correlation between fluid (Coriolis) circulation and the strength of centrifugal radial velocity. Therefore the question is now, can Stokes theorem be equated to, the third moment of fluctuating radial velocity? If this is possible, then an equation can then be derived relating axisymmetric

Coriolis circulation in rotational turbulence to the third moment of radial velocity v_r'.

Start with circulation Γ,

$$\Gamma = \oint_C \mathbf{v} \cdot d\boldsymbol{\ell} = \int_S \nabla \times \mathbf{v} \cdot d\mathbf{S} \tag{6}$$

In the annulus the circulation is dominated by the azimuthal component of velocity (v_θ):

$$\Gamma = \int_0^{2\pi} v_{\theta(r)} r \; d\theta = 2\pi r \; v_{\theta(r)} \tag{7}$$

Here $v_{\theta(r)}$ is the azimuthal velocity at radius (r).

The third moment of fluctuating radial velocity is $\overline{v_r'^3}$. To apply Gauss theorem, consider $\overline{v_r'^3}$ as a scalar field and compute its divergence:

$$\nabla \cdot \overline{v_r'^3} = \nabla \overline{v_r'^3} = \frac{\partial \overline{v_r'^3}}{\partial r} + \frac{1}{r}\frac{\partial (r\overline{v_r'^3})}{\partial \theta} + \frac{\partial \overline{v_r'^3}}{\partial z} \tag{8}$$

For an axisymmetric annulus $\frac{\partial}{\partial \theta} = 0$ due to the azimuthal cyclic (periodic) nature, and assuming no variation in the axial direction (periodic boundary condition) $\frac{\partial}{\partial z} = 0$, thus simplifies to,

$$\nabla \cdot \overline{v_r'^3} = \frac{\partial \overline{v_r'^3}}{\partial r} \tag{9}$$

Now apply Gauss theorem to the annulus:

$$\int_V \nabla \cdot \overline{v_r'^3} \; dV = \int_{\partial V} \overline{v_r'^3} \mathbf{v} \cdot d\mathbf{S} \tag{10}$$

and given the simplified divergence:

$$\int_{r_1}^{r_2} \frac{\partial \overline{v_r'^3}}{\partial r} r \; dr = \overline{v_r'^3}\Big|_{r_1}^{r_2} \tag{11}$$

To connect Γ with $\overline{v_r'^3}$ consider the relationship between the azimuthal velocity v_θ and the radial velocity v_r. In rotational turbulence, the azimuthal velocity can be influenced by radial velocity through mechanisms like vortex stretching or turbulent transport.

Assume a relationship of the form:

$$v_{\theta(r)} = f(\overline{v_r'^3}, r, t) \tag{12}$$

This function f depends on the specific dynamics of the turbulence and may involve empirical or theoretical coefficients. Given the unsteady nature of the flow, include the time derivative of (v_θ) in the circulation:

$$\frac{\partial \Gamma}{\partial t} = \frac{\partial}{\partial t}(2\pi r \; v_{\theta(r)}) \qquad \text{where} \qquad v_{\theta(r)} = f(\overline{v_r^3}, r, t) \tag{13}$$

This time dependence introduces additional terms in the governing equations that must be considered when relating Γ to $\overline{v_r'^3}$. By combing the expressions from Stokes and Gauss theorems and incorporating the relationship between v_θ and $\overline{v_r'^3}$, one can derive a relationship that links the circulation in the annulus to the divergence of the third moment of fluctuating radial velocity, accounting for unsteady effects. The final relationship will depend on the specific form of $f(\overline{v_r'^3}, r, t)$ and the boundary conditions of the annulus. It will provide a mathematical connection between the macroscopic circulation Γ and the microscopic turbulent fluctuations represented by $f(\overline{v_r'^3}, r, t)$.

Examining the quantities which are functions of fluctuating velocity from Dunstan (2020), the 1d plots which appear most likely to provide a distorting influence on the azimuthal (Coriolis) velocity, to form the corresponding v_r' skewness, are the plots for radial turbulent kinetic energy (TKE) production P_{rr}. See Appendix D. Therefore a final equation may include P_{rr} in some form. More work is required to properly establish and confirm the exact empirically verifiable form of the equation relating circulation, in rotational axisymmetric turbulence, to its third moment of fluctuating radial velocity.

5 Conclusions

A complete description of turbulence remains one of the biggest unsolved problems of classical physics. A way forward in understanding it better is to eliminate as much as possible the ambiguities surrounding its treatment in different reference frames, inertial

and non-inertial (the rotational frame). To this end the first paper Dunstan (2023) has sought to establish that azimuthal velocity can only be considered in the Coriolis (rotational frame). The current paper seeks now to confirm that centrifugal velocity is stronger in rotational turbulence and this bias should be considered going forward. An attempt has been made to derive an equation relating induced circulation in rotational turbulence to the third moment of radial velocity fluctuation but thus far only a functional relation has been derived.

Acknowledgment

Acknowledgments to The University of Warwick (PhD Research 2016-2020), Centre for Scientific Computing, for use of the HPC facilities *Tinis* and *Orac* (2017-2020). Also to HPC West Midlands for use of *Athena* (2019-2020). Thanks also to Professor Rustam Mullyadzhanov for sharing data on the rotating pipe. Acknowledgment is also made of this PhD research, sponsorships: The Commonwealth Scholarships Commission and The Papua New Guinea University of Technology (current location).

Appendix

A Proof of the invariance of fluctuating velocity, from Speziale 1979 Speziale (1979)

A.1 velocity decomposition

The velocity field $\mathbf{v}$ is decomposed into the mean and fluctuating parts respectively,

$$\mathbf{v} = \bar{\mathbf{v}} + \mathbf{u}$$

where ensemble mean,

$$\bar{\mathbf{v}} = \lim_{n\to\infty} \frac{1}{N} \sum_{\alpha=0}^{\infty} v^{(\alpha)}$$

where an average is taken over N experiments with the same initial and boundary conditions. The superscript α denotes the experiment under consideration. By definition the Reynolds stress tensor τ is given as,

$$\tau_{kl} = -\rho\overline{u_k u_l} \tag{14}$$

We now show that $\boldsymbol{\tau}$ is frame indifferent, i.e. $\boldsymbol{\tau}$ transforms as,

$$\boldsymbol{\tau}^* = \mathbf{Q}\boldsymbol{\tau}\mathbf{Q}^T \tag{15}$$

where the superscript T denotes the transpose. Under arbitrary time dependent rotations and translations of the spatial frame of reference $\mathbf{x}$ and shifts in the origin of time t given by,

$$\mathbf{x}^* = \mathbf{Q}(t)\mathbf{x} + \mathbf{b}(t), \qquad t^* = t + c \tag{16}$$

Here c is any constant, $\mathbf{b}(t)$ is any time dependent vector, and $\mathbf{Q}(t)$ is any time dependent orthogonal tensor so that,

$$\mathbf{Q}\mathbf{Q}^T = \mathbf{Q}^T\mathbf{Q} = \mathbf{I}, \qquad |\mathbf{Q}| = 1$$

The proof of 15 is straightforward from 14 we have,

$$\tau_{kl} = -\rho \lim_{n\to\infty} \frac{1}{N} \sum_{\alpha=1}^{N} u_k^{(\alpha)} u_l^{(\alpha)} \tag{17}$$

where,

$$\mathbf{u}^{(\alpha)} = \mathbf{v}^{(\alpha)} - \bar{\mathbf{v}} \qquad \alpha = 1, 2, 3, \cdots N \tag{18}$$

By differentiating 16 we obtain the transformation rule for $\mathbf{v}$

$$v_k^* = Q_{kl} v_l + \dot{Q}_{kl} x_l + \dot{b}_k \tag{19}$$

where a dot denotes a derivative w.r.t time. However $\mathbf{Q}(t)$ and $\mathbf{b}(t)$ are independent of the experiment α since $\boldsymbol{\tau}^*$ and $\bar{\mathbf{v}}^*$ are obtained by conducting N experiments w.r.t the same $\mathbf{x}^*$ frame. Of course $\mathbf{x}$ is independent of the same α, so that from 18 we have,

$$u_k^* = Q_{kl} v_l + \dot{Q}_{kl} x_l + \dot{b}_k - \lim_{n\to\infty} \frac{1}{N} \sum_{\alpha=1}^{N} \left(Q_{kl} v_l^{(\alpha)} + \dot{Q}_{kl} x_l + \dot{b}_k \right) \tag{20}$$

After removing those terms that are independent of α from under the summation sign we get,

$$u_k^* = Q_{kl} v_l - Q_{kl} \lim_{n\to\infty} \frac{1}{N} \sum_{\alpha=1}^{N} v_l^{(\alpha)} = Q_{kl} u_l \tag{21}$$

Which proves the fluctuating velocity $\mathbf{u}$ is frame indifferent.

Now since for the continuity equation we have $\rho^* = \rho$ we have,

$$\tau_{kl}^* = -\rho^* \lim_{n\to\infty} \frac{1}{N} \sum_{\alpha=1}^{N} u_k^{*(\alpha)} u_l^{*(\alpha)} = -\rho \lim_{n\to\infty} \frac{1}{N} \sum_{\alpha=1}^{N} \left(Q_{km} u_m^{(\alpha)} Q_{ln} u_n^{(\alpha)} \right) \tag{22}$$

Since $\mathbf{Q}(t)$ is independent of the experiment α, we have,

$$\tau_{kl}^* = Q_{km} Q_{ln} \left(-\rho \lim_{n\to\infty} \frac{1}{N} \sum_{\alpha=1}^{N} u_m^{(\alpha)} u_n^{(\alpha)} \right) = Q_{km} Q_{ln} \tau_{mn} \tag{23}$$

Which completes the proof.

B In tandem plots for comparison

B.1 Turbulent rotating pipe

Note grid independence tests and validation carried out in Dunstan (2020, 2023) show that the pipe has achieved a good level of stationarity.

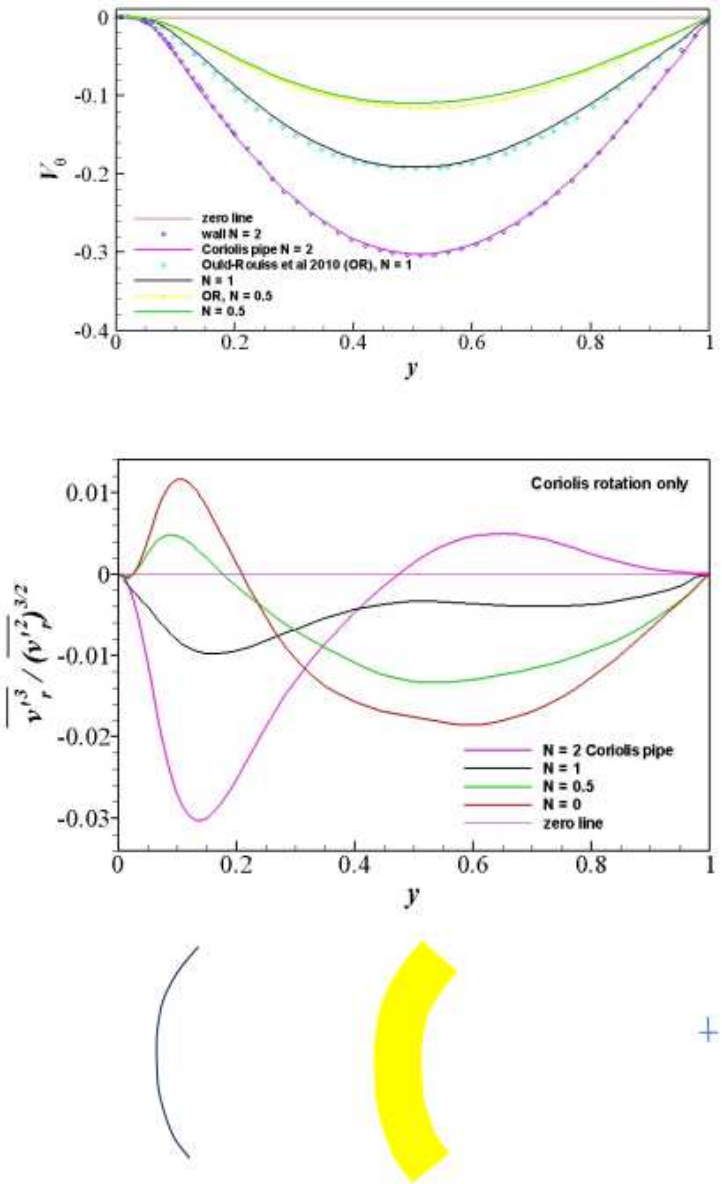


Figure 6: THE TURBULENT PIPE WITH ROTATION: The top plot is azimuthal Coriolis velocity. The middle plot is the third moment of $v_r^{'}$. The bottom plot gives an appreciation of the pipe wall and the yellow streak gives the approximate zone of peak V_θ.

B.2 Turbulent concentric pipe with inner wall rotating

Note grid independence tests and validation carried out in Dunstan (2020, 2023) show that the concentric pipe with inner wall rotating, has achieved a well developed level of stationarity.

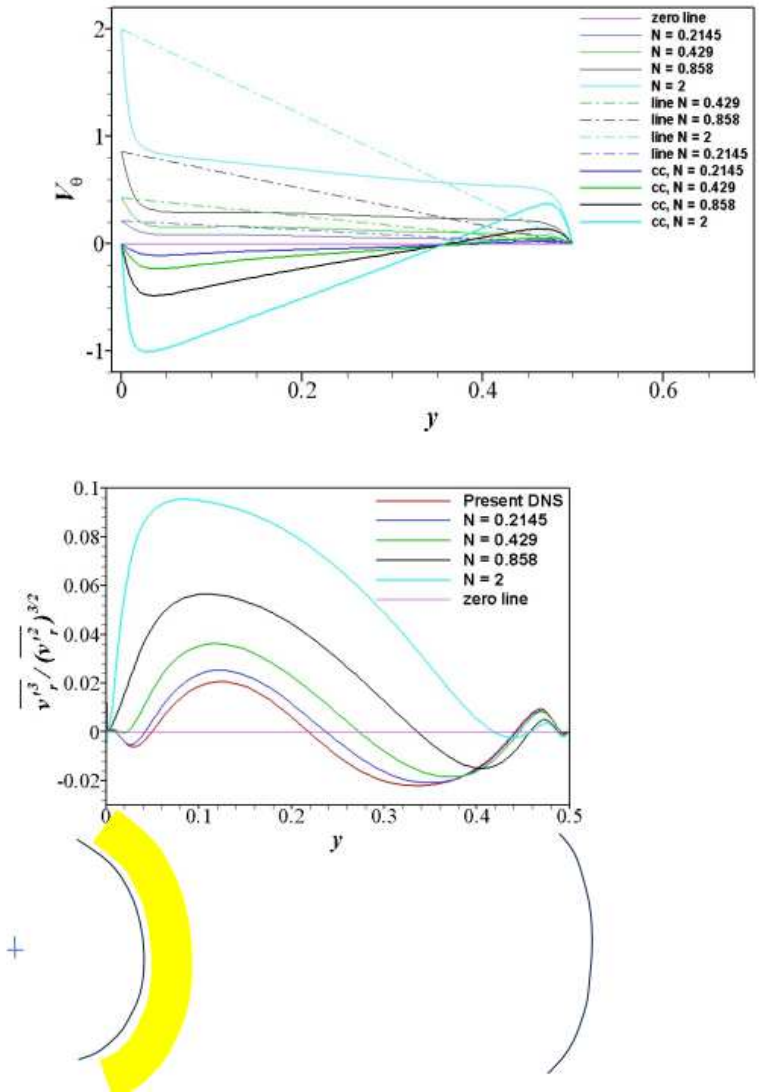


Figure 7: THE TURBULENT CONCENTRIC PIPE WITH INNER WALL ROTATION: The top plot is azimuthal Coriolis velocity. The middle plot is the third moment of $v_r^{'}$. The bottom plot gives an appreciation of the inner wall, outer wall and the yellow streak gives the approximate zone of peak V_θ, near the inner rotating wall.

B.3 Turbulent concentric pipe with outer wall rotating

Note grid independence tests and validation carried out in Dunstan (2020, 2023) show that the concentric pipe with outer wall rotating has not achieved stationarity and the flow is still developing. Regardless some results are placed here in the Appendix for comparison purposes.

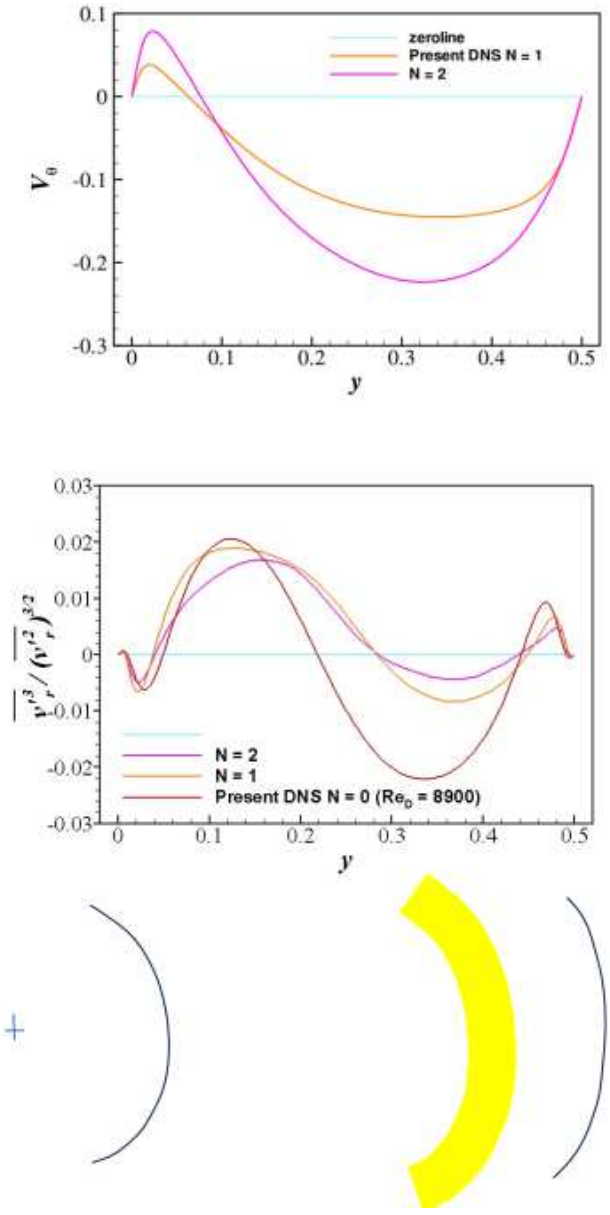


Figure 8: THE TURBULENT CONCENTRIC PIPE WITH OUTER WALL ROTATION: The top plot is azimuthal Coriolis velocity. The middle plot is the third moment of $v_r^{'}$, here positive is wall-normal outward from the inner wall (centrifugal). The bottom plot gives an appreciation of the inner wall, outer rotating wall and the yellow streak gives the approximate zone of peak V_θ.

C DNS of Channel flow - skewness plot

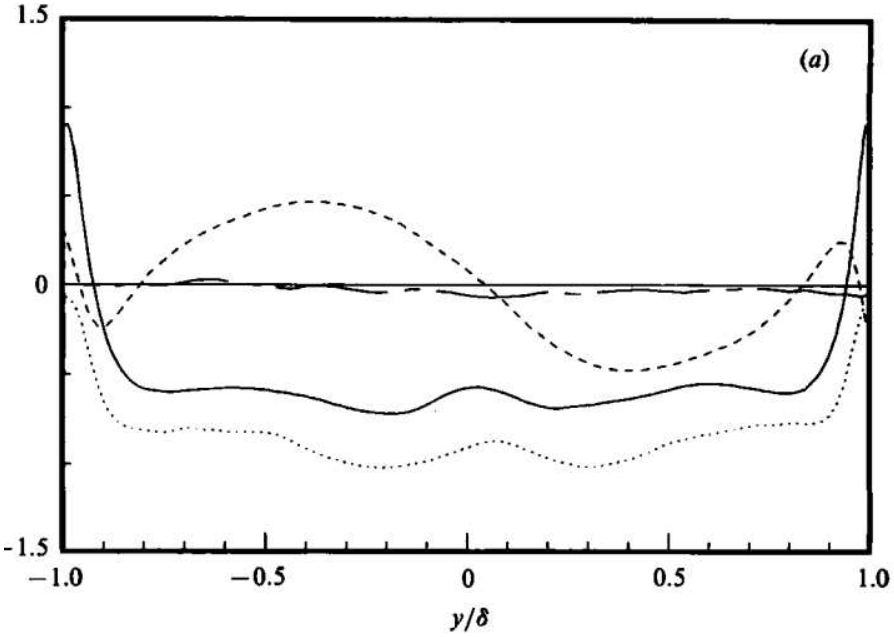


Figure 9: The skewness plots from the Channel DNS experiment of Kim, Moin and Moser 1987 Kim et al. (1987). The dashed line is $S(v^{'})$, the third moment of fluctuating wall-normal(away from bottom wall) velocity, which is comparable to that in concentric pipe without wall rotation ($N = 0$).

D Turbulent statistics for the radial component of turbulent kinetic energy production P_{rr}.

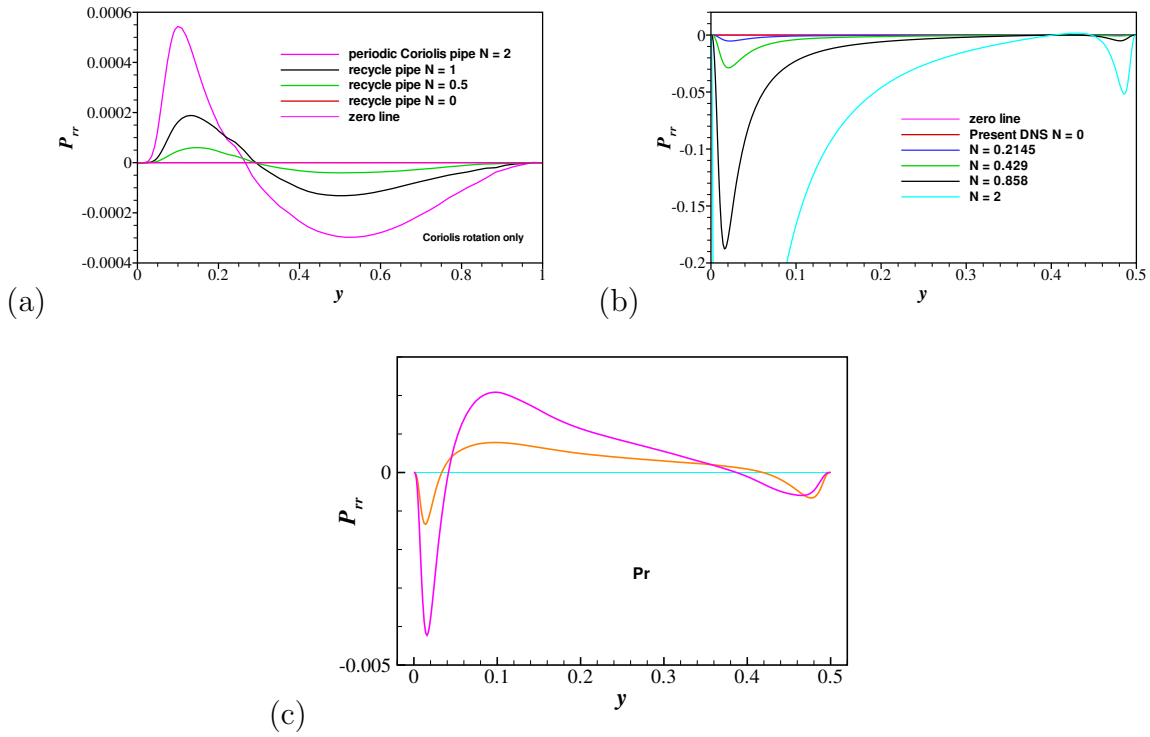


Figure 10: Radial component of turbulence production in the (a) *pipe with rotation*, (b) *concentric pipe with inner wall rotation*, (c) *concentric pipe with outer wall rotation*.

The equation for the radial component of TKE production, as taken from Dunstan (2020), is given as,

$$P_{rr} = \overline{v_r'^2} = 2\overline{v_\theta' v_r'}\frac{\partial V_\theta}{\partial r} + \underline{2\overline{v_\theta' v_r'}\left(\frac{V_\theta}{r}\right)}$$

Here, the term that is not underlined is sometimes deemed too small and is left out.

References

D. Barkley. A fluid mechanics analysis of the teacup singularity. *Proceedings of the Royal Society of London A*, 476(2240):20200348, 2020.

S. Y. Chung and H. J. Sung. Large eddy simulation of turbulent flow in a concentric annulus with rotation of an inner cylinder. *International Journal of Heat and Fluid Flow*, 26(2):191–203, 2005.

S. D. Dunstan. *DNS of convective rotational turbulence in the pipe, concentric pipe and jet*. PhD thesis, School of Engineering, University of Warwick, UK, November 2020.

S. D. Dunstan. A direct numerical simulation display of the rotational frame preference of turbulence. *AIP Advances*, 13:045216, 2023.

P. F. Fischer, J. W. Lottes, and S. G. Kerkemeir. Nek5000 user documentation, 2008. URL `https://nek5000.mcs.anl.gov/`.

K. Kikuyama, M. Murakami, K. Nishibori, and K. Maeda. Flow in an axially rotating pipe - (A calculation of flow in the saturated region). *Bulletin of the JSME*, 26(214): 506–513, 1983.

J. Kim, P. Moin, and R. Moser. Turbulence statistics in fully developed channel flow at low Reynolds number. *Journal of Fluid Mechanics*, 177:133–166, 1987.

R. Mullyadzhanov, S. Abdurakipov, and K. Hanjalic. Helical structures in the near field of a turbulent pipe jet. *Flow, Turbulence and Combustion*, 98(2):367–388, 2017.

P. Orlandi and M. Fatica. Direct simulations of turbulent flow in a pipe rotating about its axis. *Journal of Fluid Mechanics*, 343:43–72, 1997.

M. Ould-Rouiss, A. Dries, and A. Mazouz. Numerical predictions of turbulent heat transfer for air flow in rotating pipe. *International Journal of Heat and Fluid Flow*, 31 (4):507–517, 2010.

G. Reich and H. Beer. Fluid flow and heat transfer in an axially rotating pipe - 1. Effect of rotation on turbulent pipe flow. *International Journal of Heat and Mass Transfer*, 32(3):551–562, 1989.

C. G. Speziale. Invariance of turbulence closure models. 22(6):1033–1037, 1979.

X. Wang. *Direct numerical simulation of turbulent pipe flow with* 90° *bends*. PhD thesis, School of Engineering, University of Warwick, UK, September 2017.

A. White. Flow of a fluid in an axially rotating pipe. *Journal of Mechanical Engineering Science*, 6(4), 1964.